Accepted Manuscript

Water-based fractionation of a commercial humic acid. Solid-state and colloidal characterization of the solubility fractions

Weronika M. Swiech, Ian Hamerton, Huang Zeng, David J. Watson, Eleonore Mason, Spencer E. Taylor

Water-based fractionation of a commercial humic acid. Solid-state and colloidal characterization of the solubility fractions.

Weronika M. Swiech[a], Ian Hamerton[b,1], Huang Zeng[c], David J. Watson[b],

Eleonore Mason[d], and Spencer E. Taylor[a]*

[a] Centre for Petroleum and Surface Chemistry, Department of Chemistry, Faculty of Engineering and Physical Sciences, University of Surrey, Guildford, Surrey GU2 7XH, UK

[b] Department of Chemistry, Faculty of Engineering and Physical Sciences, University of Surrey, Guildford, Surrey GU2 7XH, UK

[c] BP America, Upstream Technology, 501 Westlake Blvd., Houston TX 77079, USA

[d] Department of Chemistry, University of Reading, Reading, RG6 6AD

Email: s.taylor@surrey.ac.uk

Abstract

Background and hypothesis. Humic acid (HA) is of considerable environmental significance, being a major component of soil, as well as being considered for application in other technological areas. However, its structure and colloidal properties continue to be the subject of debate, largely owing to its molecular complexity and association with other humic

---

[1] Current address: Bristol Composites Institute (ACCIS), Department of Aerospace Engineering, Queen's Building, University of Bristol, University Walk, Bristol, BS8 1TR

1

substances and mineral matter. As a class, HA is considered to comprise supramolecular assemblies of heterogeneous species, and herein we consider a simple route for the separation of some HA sub-fractions.

Experiments. A commercial HA sample from Sigma-Aldrich has been fractionated into two soluble (**S1**, **S2**) and two insoluble (**I1**, **I2**) fractions by successive dissolution in deionized water at near-neutral pH. These sub-fractions have been characterized by solution and solid-state approaches.

Findings. Using this simple approach, the HA has been shown to contain non-covalently bonded species with different polarity and water solubility. The soluble and insoluble fractions have very different chemical structures, as revealed particularly by their solid-state properties (^{13}C NMR and IR spectroscopy, and TGA); in particular, **S1** and **S2** are characterized by higher carbonyl and aromatic contents, compared with **I1** and **I2**. As shown by solution SAXS measurements and AFM, the soluble fractions behave as hydrophilic colloidal aggregates of at least 50 nm diameter.

Keywords

AFM, colloidal properties, humic acid fractionation, IR spectroscopy, solid-state NMR, surface tension, SAXS, TGA, zeta potential

1. Introduction

The present paper considers the aqueous solubility and composition of a commercial sample of humic acid (HA). This has been chosen as an example of one of the classes of "humic substances" produced by the environmental decomposition of natural organic matter, and which are loosely defined in terms of the procedures used in their extraction. Humic substances are present in soils, rivers and other aquifers, and HAs have been shown to exist as aggregates of colloidal size at sufficiently high concentration [1,2]. Our original interest in these materials stems from their role in bitumen extraction from oil sand ores [3,4], where HA is mostly complexed with clays which, depending on the geological origin, can have different consequences for bitumen recovery [5,6]. However, the present work has a more general context.

On a molecular level, HAs are difficult to characterize. They are known to be (or contain) polyelectrolytes which interact strongly with certain cations to form insoluble complexes [7,8], and have been shown to be active in removing metal contaminants from water [9]. Other studies have demonstrated an improved ability of humic substances over conventional surfactants, such as Triton X-100 or sodium dodecyl sulfate, to aid soil bioremediation through the removal of pollutants such as polyaromatic hydrocarbons, thiophenes, sulfones or biphenyls [10].

As has recently been discussed [11], humic substances have been subdivided into three separate classes based on their respective solubility characteristics. Thus, humins are insoluble under alkaline conditions, fulvic acids are soluble throughout the pH range, and HAs are insoluble under acidic conditions. These materials have intrinsic surfactant-like

3

tendencies, e.g. reducing the surface tension of aqueous solutions [2,12-14] and solubilizing organic molecules in colloidal aggregates [15].

The separation of humic substances has been the subject of a number of studies, as recently reviewed [16]. The analysis of different fractions taken from within individual classes has only served to highlight the molecular complexity of these substances, and detailed molecular structures still remain elusive. Indeed, this may not be surprising based on the arguments that humic substances are more likely to be a "continuum of progressively decomposing organic compounds" than "inherently stable and chemically unique compounds" [11].

In this paper, we are particularly interested in the composition and colloidal properties of HA component species. In the majority of previous studies, chemical and molecular size differences have been exploited in order to effect fractionation. For example, the recent procedure used by Chilom et al. [13] involved alkali- and solvent-based extractions, enabling the isolation of one lipid-like and two humic-like fractions. Powell and Town solubilized HAs using a combination of pH and different ionic media which were then fractionated based on molecular size using gel permeation chromatography combined with equilibrium dialysis [17]. Conte et al. used preparative size exclusion chromatography to produce seven fractions from a lignite HA which were shown by different spectroscopic analyses to vary in aromatic-aliphatic character and oxidized state [18]. Using ultrafiltration, Carlsen et al. produced six molecular size fractions ranging from <1 kDa to <100,000 kDa from Aldrich HA and examined their respective interactions with Eu^{3+} ions [19]. Similarly, Francioso et al. produced six fractions from Na humate solution ranging from 5-10 kDa to >300 kDa using tangential ultrafiltration, which were characterized by vibrational and NMR spectroscopic techniques [20].

4

However, Pitois et al. [21] used a different approach to produce "chemical adsorptive" fractions from commercial HA by adsorption on quartz sand. They found that adsorption of HA was a two-stage process, one occurring faster (~3 h) than the other (~45 h). The HA solutions remaining after each adsorption period were analyzed using asymmetric flow-field flow fractionation coupled with UV/visible absorption spectrophotometry, which showed that adsorption of lower molecular weight components (<4800 Da) occurs initially, followed by higher molecular weight components (1400-9200) [21]. Fractions produced by this method are clearly towards the lower molecular weight end of the ultrafiltration fraction ranges.

A contemporary model for the structure of HAs proposes supramolecular assemblies of smaller heterogeneous molecules held together by hydrophobic interactions and hydrogen bonding [22,23]. The composition of humic substances, including HA, are naturally heterogeneous and source-dependent, since they originate from the breakdown of plant and animal matter by microbiological and abiotic transformation.

Herein, we present results from an experimental study on a commercial HA sample from Sigma-Aldrich which has been the subject of several reports in the literature over the years [1,7,9,12,21]. We report that it is possible to isolate "solubility fractions" based on differential solubility in deionized water under near-neutral pH conditions. Klučáková and Pekař [24,25] have previously noted different dissolution/solubility characteristics of solid HAs, including a commercial sample from Fluka, which on the basis of its pH-concentration behavior is considered similar to the product used herein (see later). These workers proposed a multi-step dissolution mechanism upon interaction with water, involving dissolution, with or without acid dissociation [24,25]. We were therefore interested to investigate further the water solubility of the commercial HA and the nature of the solubility fractions produced.

5

2.   Experimental
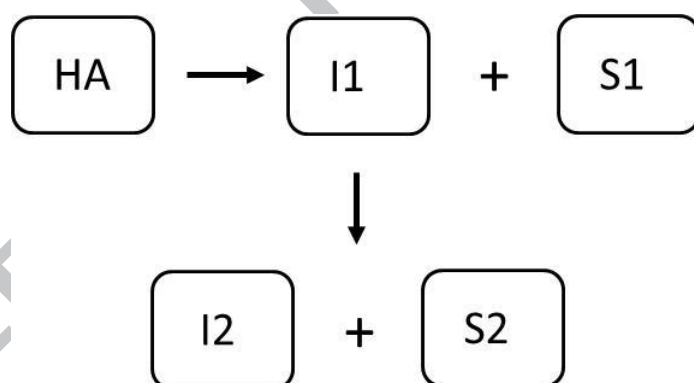
2.1. Materials and HA fractionation in water

All reagents, including neutral HA, the corresponding sodium salt (NaHA), the inorganic salts NaCl, $CaCl_2.2H_2O$ and $LaCl_3.7H_2O$, and cetyltrimethylammonium bromide (CTAB) were the highest purity grades available from Sigma-Aldrich, UK and were used as received. Aqueous solutions were prepared using deionized water (resistivity 18.2 MΩ.cm) from a Millipore Direct-Q system.

Inorganic matter is known to be an impurity in HA and this is confirmed by the lower elemental compositions in the present sample of HA compared with the literature values of a similar product produced from NaHA: found (lit. [26]) (%): C, 36.9 (49.7); H, 3.10 (4.49); C/H ratio 0.99 (0.92). On the other hand, the similar C/H ratio found for the present unpurified product is consistent with an impurity devoid of carbon and hydrogen. Thermal analysis data are reported later in this paper. Since the compositions of HA and NaHA could potentially vary from sample to sample, experiments were conducted as much as possible using a single commercial batch (identified by lot number).

HA and NaHA solutions were prepared by agitating the appropriate quantities of the respective dry solids in deionized water using an orbital shaker at ambient temperature (20 ± 2 °C). Solutions of the desired concentration of the sodium salt were prepared by dissolving the exact weighed amount of NaHA in deionized water. However, in the case of HA, it was discovered that a proportion of the HA was soluble in deionized water, the concentration of the soluble fraction being dependent on the initial mass of HA, and to a lesser extent, time (from 4-48 hours used). The solutions produced in this way were then filtered to remove

6

undissolved solid (termed "insoluble 1", **I1**), and the concentrations of the soluble fraction (termed "soluble 1", **S1**) in the filtrates were determined gravimetrically after drying. Lower concentration solutions were prepared by dilution.

This procedure was extended by removing the undissolved **I1** from the first dissolution stage and adding this to fresh deionized water. This resulted in further, but also incomplete, dissolution and, again, the undissolved solid (termed "insoluble 2", **I2**) was removed by filtration, the filtrate containing the second soluble component ("soluble 2", **S2**). This procedure is shown in Scheme 1. The corresponding "soluble" components (**S1** and **S2**) were recovered by carefully drying aliquots of the respective solutions in preparation for further analysis.

Scheme 1. Sequence of humic acid dissolution in water to produce soluble (**S1**, **S2**) and insoluble (**I1**, **I2**) fractions.

2.2. Characterization Methods

2.2.1.   *Colloidal and solution analysis*

Zeta potentials of **S1** aqueous solutions (prepared by dilution of a stock solution as described above to produce solutions in the range 2.6–1320 mg/L) were determined using a

ZetaMaster (Malvern Instruments, Malvern, UK). Surface tensions of the aqueous solutions of NaHA and **S1** were determined as a function of concentration by the du Noüy ring method with a Krüss K10 tensiometer (Krüss GmbH, Hamburg, Germany). The Pt-Ir ring was rinsed thoroughly with deionized water and flamed before making each measurement, which were made at least in triplicate. Both sets of measurements were made at ambient temperature (20 $\pm$ 2 °C).

Small-angle X-ray scattering (SAXS) measurements on aqueous **S1** and **S2** solutions were made using the B21 beamline at the Diamond Light Source of the UK National Synchrotron Science Facility (Harwell Science and Innovation Campus, UK). Solutions were manually injected via a coupled syringe into a quartz capillary (1.8 mm internal diameter) in the X-ray beam. The quartz capillary was enclosed in a vacuum chamber, in order to reduce background scatter. Experiments were carried out with a camera length of 4.01 m and fixed energy (12.4 keV, corresponding to a wavelength of 0.999 Å), providing a q range of 0.022 to 4.2 nm^{-1}. Scattering patterns were acquired using a Pilatus 2M detector. Background (water) subtraction and radial averaging were performed using the dedicated beamline software ScÅtter.

Concentrations of acid groups in **S1** and **S2** were determined using a modification of the cationic surfactant-based precipitation method described by Nobili et al. [27]. In the present work, typically 5-10 mg of solid **S1** or **S2** was dissolved in deionized water (40 mL) and titrated with a solution of CTAB (i.e. CTA$^+$ Br$^-$) of known concentration ($\sim$5 $\times$ 10^{-3} M) at either pH 7 or pH 9.8. Reaction with CTA$^+$ at the former pH provides a measure of acid groups dissociated at pH 7 (mainly, but not exclusively, carboxylic), whereas at the higher pH CTA$^+$ reacts additionally with phenolic groups [27]. The original method identifies the most optically-clear supernatant, after centrifuging a range of mixtures with different HA/CTAB ratios. Here, we detect the end-point visually by the appearance of large flocs,

8

assisted by "spotting" one drop of the titration mixture onto a filter paper (Whatman #1). The presence of large flocs is apparent as dark particles (see Fig. S1, Supporting Material). We also continuously monitored the solution pH during the titration, which decreases as the end-point is approached, in a single stage at the lower pH, and in two stages at the higher pH, as also shown in Fig. S1. We suggest that the two stages indicate the types of acid groups involved [27].

The effect of ionic strength and cation valency on the dissolution of HA, and the colloid stability of **S1**, were analyzed spectrophotometrically (Thermo-Scientific Evolution 2000 UV-Vis spectrophotometer). In the former experiments, HA was suspended in NaCl, $CaCl_2$ and $LaCl_3$ solutions and agitated using an orbital shaker (4 h; 200 rpm). After filtration (Whatman #1 filter paper), the absorbance at 450 nm of each filtrate was compared with the corresponding value for a suspension of HA in deionized water. For the colloid stability measurements, aliquots (2.5 mL) of a stock **S1** solution (0.62 g/L) were mixed with equal volumes of known concentration salt solutions and also agitated using an orbital shaker (4 h; 200 rpm). In these latter experiments, any precipitate formed was removed by centrifugation (Rotina 380 Hettich benchtop centrifuge at 5000 rpm for 10 minutes), and the residual **S1** concentrations determined by comparing absorbance values at 450 nm with a deionized water reference (i.e. equivalent to 0.31 g/L).

2.2.1. *Solid-state analysis*

Thermogravimetric analysis (TGA) was conducted using a TA Instruments Q500 TGA analyzer. Powdered samples (~5 mg) were placed in a shallow platinum crucible and heated in static air at a rate of 10 K/min from room temperature to 950 ℃. The results are expressed as thermogravimetric (TG) and first derivative (DTG) plots. Elemental analyses (CHN) of the

humic substances were determined by combustion analysis using an Exeter Analytical CE440 elemental analyzer. Infrared spectroscopic analysis was carried out using a Brüker Alpha instrument in ATR mode (2 cm^{-1} spectral resolution).

Solid-state NMR experiments were conducted on HA, NaHA, **S** and **I** samples at the former EPSRC National Solid-State NMR Service facility at the University of Durham. ^{13}C Multiple cross-polarization magic angle spinning (CPMAS) spectra [28] were obtained at 100.56 MHz at ambient probe temperature using a Varian VNMRS spectrometer based on a 9.4 T Oxford Instruments superconducting magnet.

Imaging of mica surfaces containing humic acid fraction **S1** by atomic force microscopy (AFM) were obtained under ambient conditions in air using a Brüker Innova atomic force microscope in tapping mode using 256 scan lines and a scan rate of 4 Hz. The images were post-processed using Brüker NanoScope software, which was used primarily to level the images.

3. RESULTS AND DISCUSSION

3.1. Aqueous fractionation of HA

The dissolution behavior of the commercial HA powder is very different from that of NaHA. Unsurprisingly, aqueous NaHA solutions are easily prepared simply by stirring the solute into water. On the other hand, as previously also found by Klučáková and Pekař, HA is only partially soluble, even when very small quantities are added to water under neutral pH conditions [24,25]. Here, we have found that proportionately more concentrated solutions were produced by increasing the initial quantities of HA powder, and even after prolonged

(~48 h) agitation the water/HA mixtures contained undissolved (organic and inorganic) components.

As an example, the addition of as-received HA powder (0.125 g) to deionized water (100 mL) at ambient temperature consistently produced a concentration of 0.39 ± 0.03 g/L in solution, suggesting the presence of ~30% of a soluble component (**S1**) under these conditions. The concentration increased to 0.50 and 0.54 g/L at 50° and 80° C, respectively. Extending the number of ambient temperature experiments produced the data shown in Fig. 1(a). During dissolution, the pH was neutral to slightly acidic, and changed little with time, as noted elsewhere for another commercial HA sample [25]. Over the course of a 4 h experiment in which 2 g HA was suspended in deionized water (100 mL), the pH of the solution decreased slightly from 6.11 to 6.02, while for an initial suspension of 6 g HA in the same volume of deionized water, the pH remained at 5.74 throughout. The removal of excess undissolved solid (i.e. **I1**, Scheme 1) by filtration or centrifugation enabled **S1** solutions of relatively high concentration to be obtained.

The data in Fig. 1(a) indicate that a steady linear increase in the **S1** concentration is seen as a function of the initially suspended HA, which indicates a limiting solubility for the HA components comprising **S1** under these conditions. **S1** could potentially exist in a dissolved state or in colloidal suspension, and coupled with the solubility behavior, led us to consider the compositional and solution properties of the soluble and insoluble fractions.
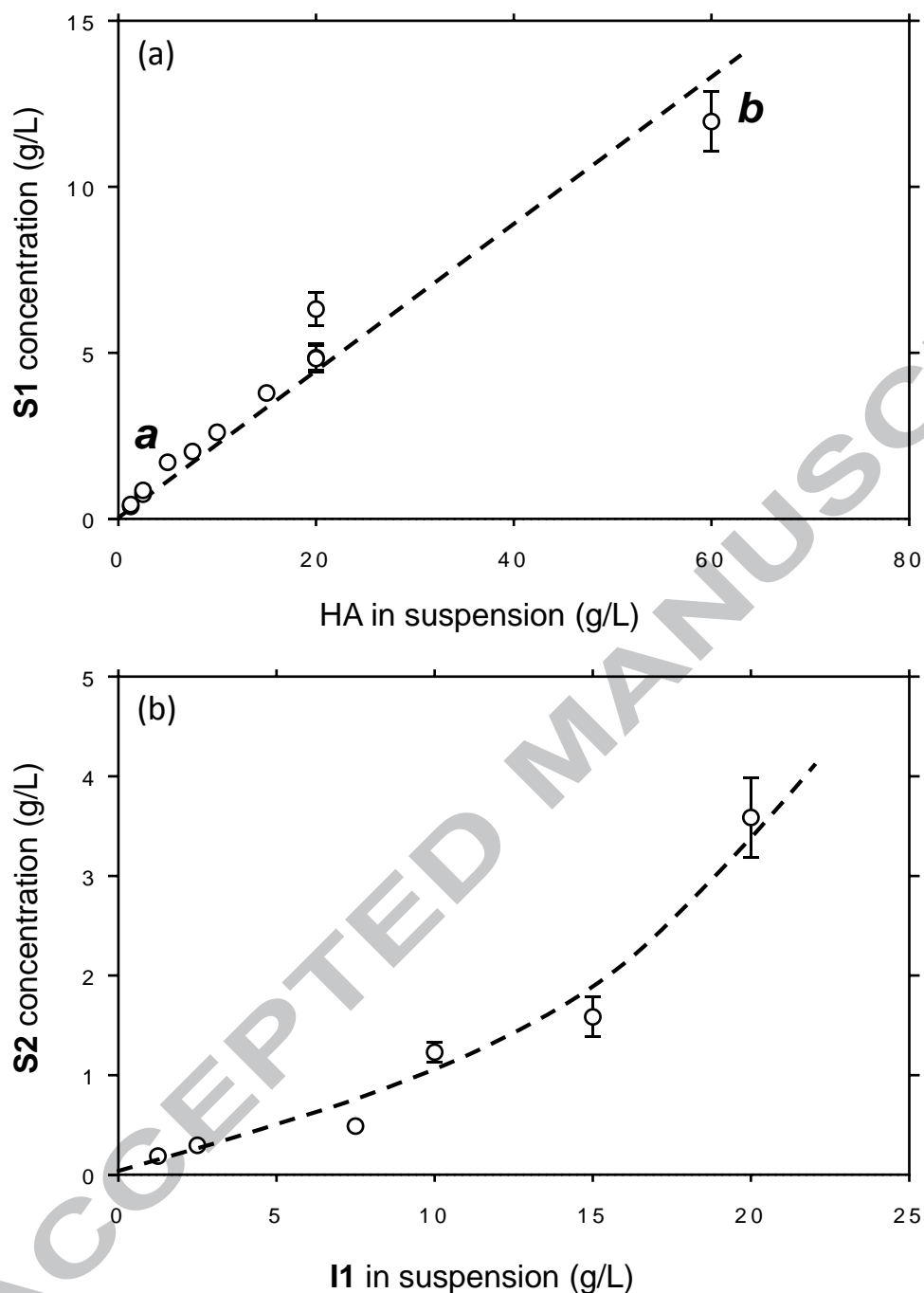
Fig. 1. (a) Dissolution of HA powder in deionized water to produce **S1** in solution, leaving insoluble **I1**. The two highlighted points (*a* and *b*) identify the **S1** solutions used to produce samples for AFM. (b) Plot showing the solubility of excess powdered **I1** deionized water to yield **S2**. The curves are drawn to guide the eye.

Upon isolating the separated insoluble HA fraction **I1** (see Scheme 1), it was also found to

yield ~30% of a second soluble fraction **S2** when added to further (100 mL) deionized water;

filtration also produced another residual insoluble fraction **I2**. The **S2** concentration is plotted in Fig. 1(b) as a function of the original suspended **I1** concentration, from which it can be seen by comparison with Fig. 1(a) that dissolution is generally lower than for HA. This is indicative of a selective dissolution process, and the differences in the fractions from successive dissolution steps would be expected to reflect the respective hydrophilicity of the different fractions.

3.2 Compositional and functional analysis of HA and fractions

Thermogravimetric analysis (TGA) has been shown to be a useful technique for characterizing HAs and other humic substances in past studies [29,30]. The pattern of HA decomposition of a standard Suwannee River humic acid, for example, shows a small mass loss in the region of 300–400 °C followed by a larger mass loss between 450–550 °C [29]. Below ~400 °C, mass loss is generally a result of decomposition or elimination of oxygen-containing functional groups, whereas above 400 °C it reflects the high aromatic content [29]. Here, TGA in air has been performed on the fractions **S1**, **S2**, **I1** and **I2** as well as the precursor HA. As can be seen in Fig. 2, the TG and DTG profiles for the two soluble fractions are similar, as are those for the two insoluble fractions, although the respective behaviors of soluble and insoluble fractions are distinctly different; the profile for the original HA is intermediate.

All the samples show ~10-15% mass loss up to ~300 °C, most probably a result of dehydration. However, true thermal degradation first appears as a small peak in the derivative plots at ~300-325 °C for HA and the insoluble fractions, each amounting to ~10% mass loss. The main degradation peaks for **I1** and **I2** follow at 423 and 390 °C, respectively, compared with 555 °C for HA. The widths of these peaks decrease in the order HA > **I1** > **I2**, which may reflect decreasing sample heterogeneity.

13

On the other hand, degradation of **S1** and **S2** is entirely different, exhibiting much higher thermal stability. In these fractions, a steady mass loss totaling ~15% occurs up to 600 °C. This is followed by the most significant mass loss (~45%) in the range 600-900 °C, which contains two main degradation peaks at 784 and 890 °C for **S1**, and 754 and 832 °C for **S2**, indicative of char formation from aromatic structures; oxidation subsequently occurs at much higher temperatures.

HA, **I1** and **I2** each produce ~25-33% residue (note that the HA supplier quotes ~20 % ash), whereas the corresponding yields from **S1** and **S2** are approximately half these values (see Table 1). A more detailed comparison of the DTG plots in Fig. 2(b) reveals that degradation of the original HA contains minor contributions from each of the individual fractions. A broad peak at ~800 °C, for instance, is an indication of the soluble fractions, whereas the insoluble fractions are more apparent in the temperature region leading up to the main HA degradation at ~550 °C. However, it is interesting to note that the responses of the respective fractions are not reflected in the overall behavior of HA. By considering the TG/DTG profiles for the HA/**S1** and **I1**/**S2** solubility pairs, it appears that char formation in the soluble fractions is suppressed by the presence of the respective insoluble fractions – for example, mass loss from HA at >600 °C is 5.8% whereas it is 50.3% in **S1**, and yet HA contains ~30% **S1**.

Table 1. Microanalytical and TGA residue data and calculated atomic ratios for HA and its fractions.

	C (wt%)	H (wt%)	N (wt%)	C/H atomic ratio	O/C atomic ratio[a]	Residue from TGA (%)
HA[b] Batch 1 (Lot # BCBG7429V)	40.33	3.69	0.80	1.10	0.40	33.9
Batch 2 (Lot # BCBK5107V)	42.75	3.61	0.99	1.01 (1.06)[c]	0.47	25.9
S1	30.5	1.64	<0.3	0.61	1.28	12.7
S2	36.9	2.20	<0.3	0.72	0.91	16.1
I1	40.5	2.90	<0.3	0.86	0.58	25.5
I2	41.8	3.03	<0.3	0.86	0.55	24.4

[a] %O calculated by difference, including residue content.

[b] Supplier's data.

[c] From ref. [31] for an earlier product dating from 1974.

The microanalytical results, summarized in Table 1, also indicate that higher TGA residue yields correspond to higher H/C atomic ratios (nitrogen levels were found to be below the 0.3% level of uncertainty of the analytical procedure). It is therefore likely that the residues contain different amounts of ash originating from the original HA, which would be retained in the insoluble fractions. Fig. 2 and Table 1 show that residue yields for HA, **I1** and **I2** are very similar, whereas the corresponding **S1** and **S2** values are significantly lower. The O/C atomic ratios, estimated by taking residue levels into account, also reveal significant polarity differences between the soluble and insoluble fractions. Being the first fraction to dissolve, it

is not surprising that **S1** has a higher relative oxygen content than **S2**, and more than double that of the insoluble fractions.
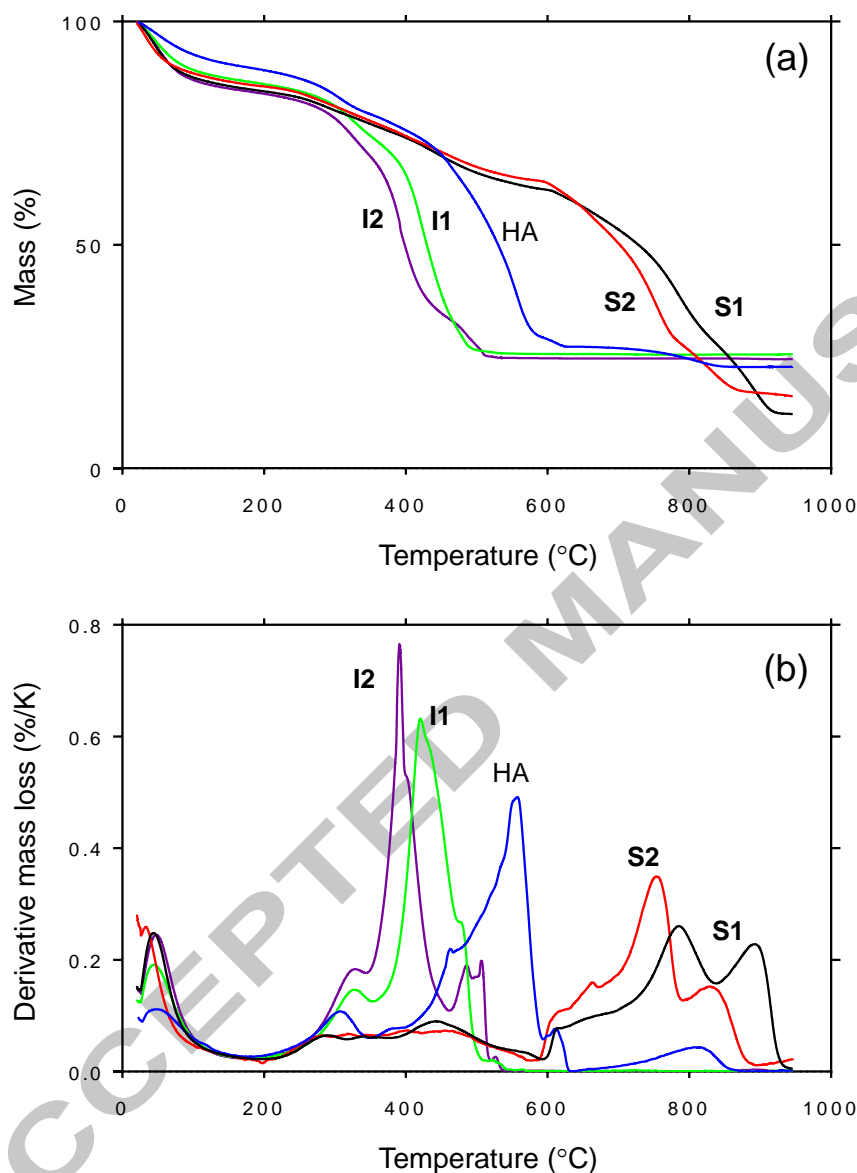

Fig. 2. (a) TG and (b) DTG profiles obtained in air for HA and the solubility fractions **S1**, **S2**, **I1** and **I2**.

Differences in oxygen content would also be expected to be evident from infrared spectroscopic analysis. Thus, Figs. 3 and S2 (Supporting Material) reveals the present HA sample and its fractions to be characteristic of a type III humic acid, based on Stevenson and

Goh's classification [32], indicating a relatively young product. In general, it is found that the main IR bands are consistent with other humic acids reported previously, and subsequent assignments follow those given in the literature [18,32-36].

All HAs contain broad bands at 3207–3356 cm^{-1} attributable to O-H stretch in both free and dimeric carboxylic groups, as well as relatively small aliphatic C-H stretching bands in the region of 2851 and 2921 cm^{-1} [32]. The spectra in Fig. S1 for HA and NaHA illustrate these features very well, the bands differing only in their relative intensities.

However, it is perhaps more pertinent to point out differences seen in the spectra for **I** and **S** fractions in the lower wavenumber region, as these are indicative of differences in chemical structure and composition. Therefore, with reference to the 900–1100 cm^{-1} region of Fig. 3, HA and all the fractions show two distinct absorption bands centered on 1021 cm^{-1}, although these are more distinctive in HA, **I1** and **I2** compared with **S1** and **S2**. These bands have previously been assigned to a C-O stretching mode in polysaccharides or polysaccharide-like substances [35,36], coinciding with Si-O stretching modes (see below), indicating that all these groups may be fewer in number in the soluble fractions, consistent with the above TGA results.

The strong band at 1563 cm^{-1} (with a very small shoulder at ∼1700 cm^{-1} in HA and the insoluble fractions), respectively assigned to C=C skeletal vibrations and C=O stretch, indicates a comparably small amount of carbonyl functionality which had been seen previously in humic acid extracted from lignite [18], and also in a commercial humic acid sample from Fluka [25]. The intensity of this band is reduced by complexation with divalent ions (Cu^{2+}, Ca^{2+}, Pb^{2+}) or salt formation with K^{+} [36]. The strong 1366 cm^{-1} band is assigned to the symmetric C=O stretch of carboxylic acid groups and C-OH stretch of phenolic groups and is slightly stronger in the soluble fractions **S1** and **S2**. A broad, lower intensity shoulder

17

at ~1250 cm^{-1} was previously assigned to the C-O stretch of esters, ethers and phenols in the humic acid structure [37]. From these comparisons, it appears that some part of the supramolecular structure of HA has partially dissolved to generate the soluble fractions. In the low wavenumber region of the spectra, a band at 531 cm^{-1}, due to Si-O-Si bending vibrations, is present in the original HA, **I1** and **I2**, but absent in **S1** and **S2**. This band is accompanied by Si-O stretching vibrations at 1030 cm^{-1} [38]. The substantial loss of those peaks in **S1** and **S2** indicates that siliceous mineral matter (discussed above as being a known impurity) most likely accumulates in the **I1** and **I2** fractions, or may be present, in part, as a separate colloidal fraction.
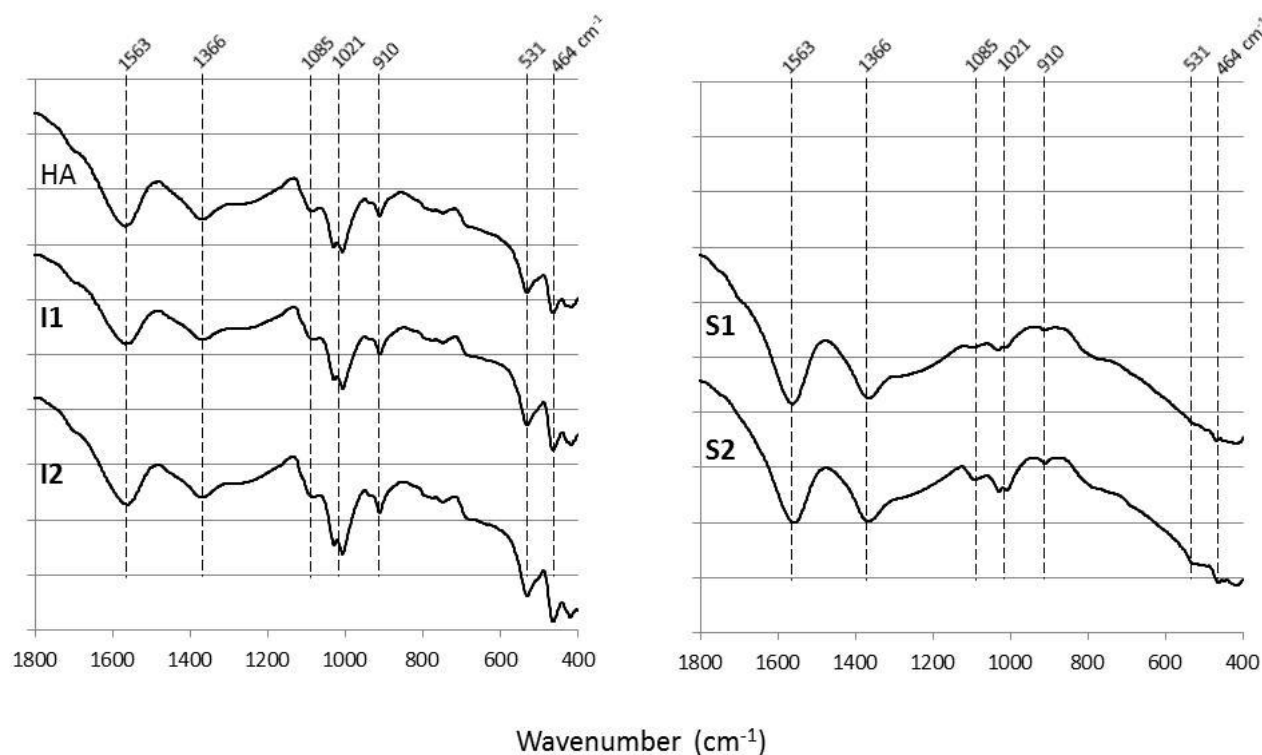

Fig. 3. ATR-IR spectra of original HA and its soluble and insoluble fractions (indicated). Arbitrary, but constant, vertical transmittance scale.

CPMAS solid-state NMR spectra of HA and its fractions, shown in Fig. S3 (Supporting Material), are in general support of the foregoing. Peaks in solid-state ^{13}C NMR spectra are typically assigned as [39-41]: alkyl C (0–45 ppm), O-alkyl C (45–110 ppm), olefinic or H- or

alkyl-substituted aromatic C (110–140 ppm), O- or N-substituted aromatic (mainly phenolic) C at 140–160 ppm, and carbonyl C (160–220 ppm). All the spectra in Fig. S3 show three main regions, corresponding to aliphatic, aromatic and carbonyl groups, as seen previously in solution spectra [42], and agree well with Aldrich HA samples studied by others [31], even after considerable purification stages to remove insoluble organic and inorganic contaminants [40,43,44]. In an extreme case, Fuentes et al. [39] obtained a spectrum almost devoid of aromatic signals which was similar in appearance to the lipid-like HA fraction extracted by Chilom et al. [13].

The present spectra allow relative signal intensities to be determined for the aliphatic, aromatic and carbonyl group regions, and these are summarized in Table 2, from which it is evident that the structural components are similar in the soluble and insoluble fractions, but that their relative intensities are noticeably different. In particular, the aliphatic/aromatic ratio for the soluble fractions is double that found for the insoluble fractions. The same is true for the respective carbonyl contents, which is consistent with the higher water solubility of **S1** and **S2**. The overall aromatic content of the soluble fractions is ~30% higher than in the insoluble fractions. These features have not been described previously with respect to fractionation studies of this commercial HA.

Table 2. Compositional data, expressed as intensity ratios, from ^{13}C CPMAS spectra for humic acid and its fractions.

Sample	$I_{Carbonyl/Total\ C}$	$I_{Aromatic\ C/Aliphatic\ C}$	$I_{Aromatic\ C/Total\ C}$
HA	0.15	1.14	0.53
S1	0.19	1.99	0.67
S2	0.20	1.92	0.66
I1	0.12	1.00	0.50
I2	0.08	0.99	0.50

3.3. Solution and colloidal properties of the S1 fraction

The aqueous behavior of humic substances is highly dependent on the presence of carboxylic and phenolic groups, which principally define their acid-base characteristics [2,11,16,24,25,27]. In the present study we have separated two water-soluble fractions by dissolution in the pH range 5.7-7. Under these pH conditions, the more acidic carboxylic acid groups will be ionized.

In Table 3 are shown the acid group contributions to **S1** and **S2**, in comparison with a previous analysis of a re-precipitated Aldrich HA [27]. From these data, it is apparent that the two soluble fractions have a similar total number of acid groups, although **S2** has a greater contribution from weaker groups, which is in accord with their respective dissolution behavior, although it is not manifest in the NMR results.

Table 3. Analysis of acid groups of S1 and S2 by precipitation with CTA$^+$. The literature data [27] have been included for comparison.

Sample	Acid groups (mmol/g)		
	Strong acid groups (pH 7)	Total acid groups (pH 9.8)	Weak acid groups
S1	2.70 ± 0.16	3.48 ± 0.03	0.78 ± 0.19
S2	2.36 ± 0.07	3.46 ± 0.02	1.10 ± 0.09
Twice re-precipitated HA (Aldrich)* from ref. [27]	2.87	3.61	0.74

Evidence for the anionic colloidal nature of the first soluble fraction comes from the effect of concentration on the zeta potential (ζ) of **S1** in water, shown in Fig. 4(a). A pH change

from 6.9 to 6.1, within the range originally used to separate **S1**, accompanies the attainment

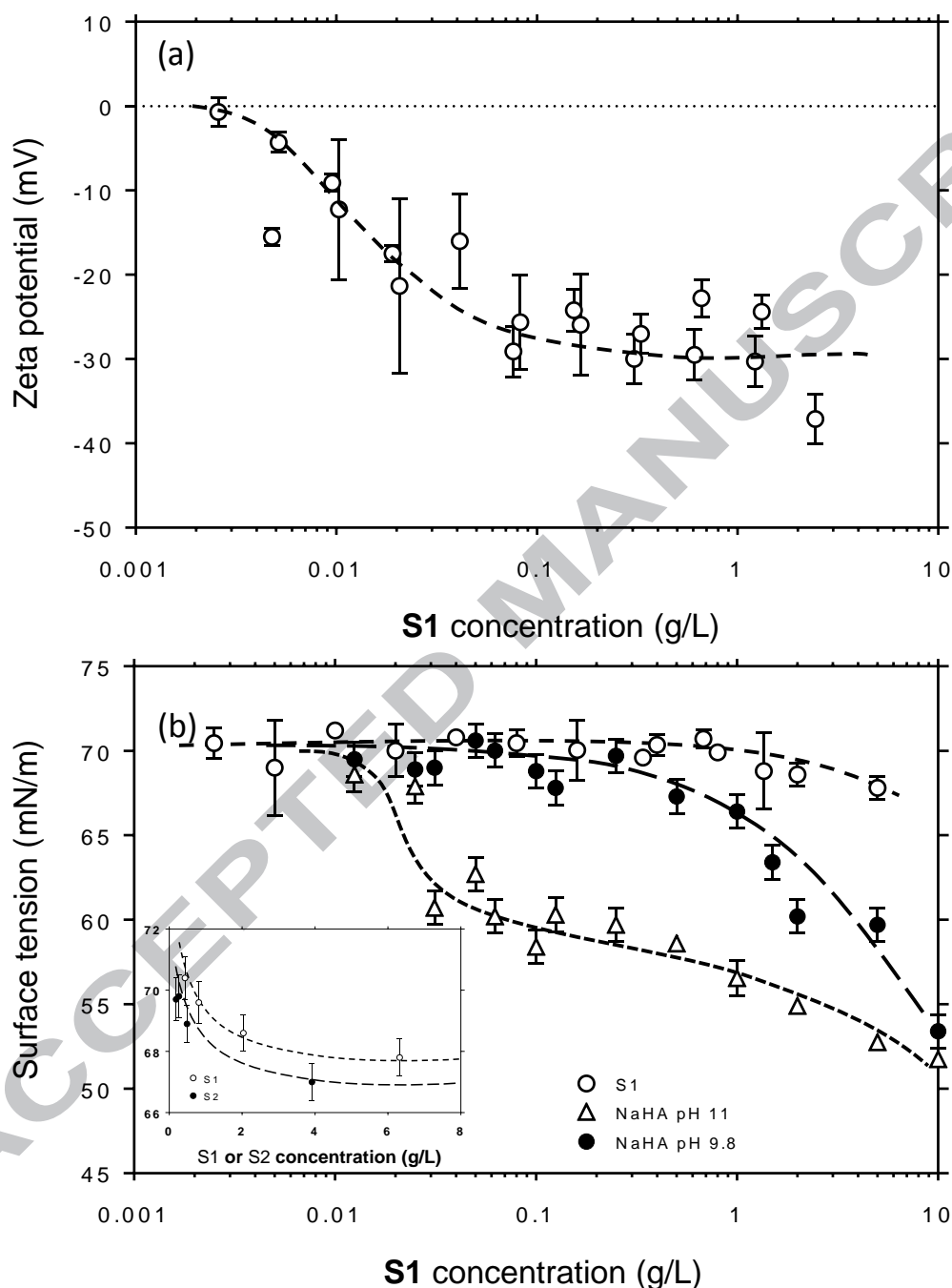of a plateau ζ of ~-30 mV, which starts at ~0.1 g/L.

Fig. 4. (a) Concentration dependence of the zeta potential for **S1** solutions. (b) Concentration dependence of the

surface tension for **S1** solutions (open circles), NaHA at their natural pH (9.8) (filled circles), and (c) NaHA at

pH 11 (open triangles). The inset shows the comparison between surface tensions for **S1** and **S2** solutions. All

lines have been drawn to guide the eye.

Corresponding surface tensions of **S1** solutions, together with NaHA (at pH 9.8 and 11), are shown as a function of concentration in Fig. 4(b). **S1** is seen to exhibit only a slight reduction in surface tension at ~3 g/L, compared with the behavior of the NaHA solutions for which the surface tension starts to decrease at ~0.3 g/L (pH 9.8) and ~0.02 g/L (pH 11). This suggests that surface activity may be related to the ionization of the phenolic groups.

The surface tension behavior of HA solutions has been determined in several previous studies from which the results were variously interpreted in terms of micelle formation [1,12,45,46], "pseudo-micelle" formation (explained as micelle-like aggregates, but without clear critical micelle concentrations) [2,47], or other "non-micelle-like" humic acid aggregates forming at high concentrations [48]. The surface tension behavior found by Terashima et al. was shown to be more dependent on HA concentration than on pH [46]. The inflection point in the surface tension-pH curve at pH ~5.5 found by these workers did not correspond to the apparent acid dissociation constant which was interpreted as reflecting the heterogeneous nature of HAs [46,49]. In fact, the data also suggested a very weak dependence on pH in the range 6-7 covered in the present study [46].

Small differences in surface tension data for the two isolated soluble fractions **S1** and **S2** at their natural pH range of 6-7 are shown in the inset to Fig. 4(b). Over the concentration range studied, **S2** is found to exhibit slightly lower surface tensions than **S1**, as would be expected from the lower solubility of the former, possibly due to the presence of lipid-like groups. In support of this, the partial solubility of humic acid [24,25] containing a lipid-like fraction (as opposed to the humic-like fraction) was previously reported to have a lower surface tension in aqueous solution [13].

3.3.1. Cation effects on HA dissolution and S1 precipitation behavior

The anionic character of **S1** is supported by the effects of metal chloride salts on HA dissolution and **S1** solubility, as shown in Fig. 5. It is seen that both properties are inhibited as cation concentrations are increased. Previous work by Powell and Town [17] indicated that humic acid solubility decreased with increasing ionic strength, i.e. salting-out upon the addition of KNO_3 (0.1 and 0.6 mol/L), $Na_4P_2O_7$ (0.1 mol/L) and synthetic seawater. These workers also reported that the effect of KNO_3 was much lower than that of $Na_4P_2O_7$ when present at the same molar concentrations. The solubility of humic acid in seawater (excluding divalent ions) decreased by ~30%. The addition of Mg^{2+} (0.05 mol/L) and Ca^{2+} (0.1 mol/L) reduced HA solubility by ~60%. From Fig. 5(a), it is seen that the ionic strengths at which each of the salts NaCl, $CaCl_2$ and $LaCl_3$ initially inhibit HA dissolution differ by approximately an order of magnitude, the multivalent cations being more effective than monovalent Na^+. This is consistent with the known preference of HA to complex with multivalent cations [19].

A minimum ionic strength can also be identified for each chloride salt, above which HA dissolution is completely inhibited. These values are in the order NaCl (~1 mol/L) >> $CaCl_2$ ≈ $LaCl_3$ (~0.03 mol/L), and most likely reflect double-layer effects as well as complexation with the HA polyelectrolyte species, since the relative ionic strengths are not fully consistent with the expected $1/z^6$ dependence on cation charge (z) predicted by DLVO theory for critical flocculation or coagulation concentrations of colloids [50]. Therefore, unlike in previous work [17], the present results suggest the importance of cation charge on dissolution through colloidal interactions and complexation, consistent with the anionic character of the HA species.

23

Similar salt effects are seen regarding the stability of **S1** solutions. As the data in Fig. 5(b) illustrate, the presence of the same three salts as above all resulted in the salting-out of **S1**. In these experiments, aliquots of stock **S1** solution (0.62 g/L) were diluted to double their volume with different concentrations of the three aqueous chloride salts. $LaCl_3$ is the most effective cation in terms of the extent of precipitation and the minimum ionic strength required. $CaCl_2$ appears to be a considerably less effective, based on the same metrics. Significantly higher ionic strength (>1 mol/L) is required to initiate precipitation in the case of NaCl. It was also qualitatively observed that **S1** precipitation rates appear to vary in the order $NaCl < CaCl_2 < LaCl_3$, suggesting that kinetic effects may also contribute to the measured precipitation. Since it is known that HA hydroxyl, carbonyl and carboxylic acid functional groups can participate in complex formation with divalent ions such as Cu^{2+}, Pb^{2+} and Ca^{2+} [36], it is possible that such reactions could also contribute to the differences shown in Fig. 5(b), rather than solely colloidal, double-layer (charge neutralization) effects [51]. The increased binding of higher valence cations to HA has been identified by other workers [19,52], and utilized in metal ion extraction [53].
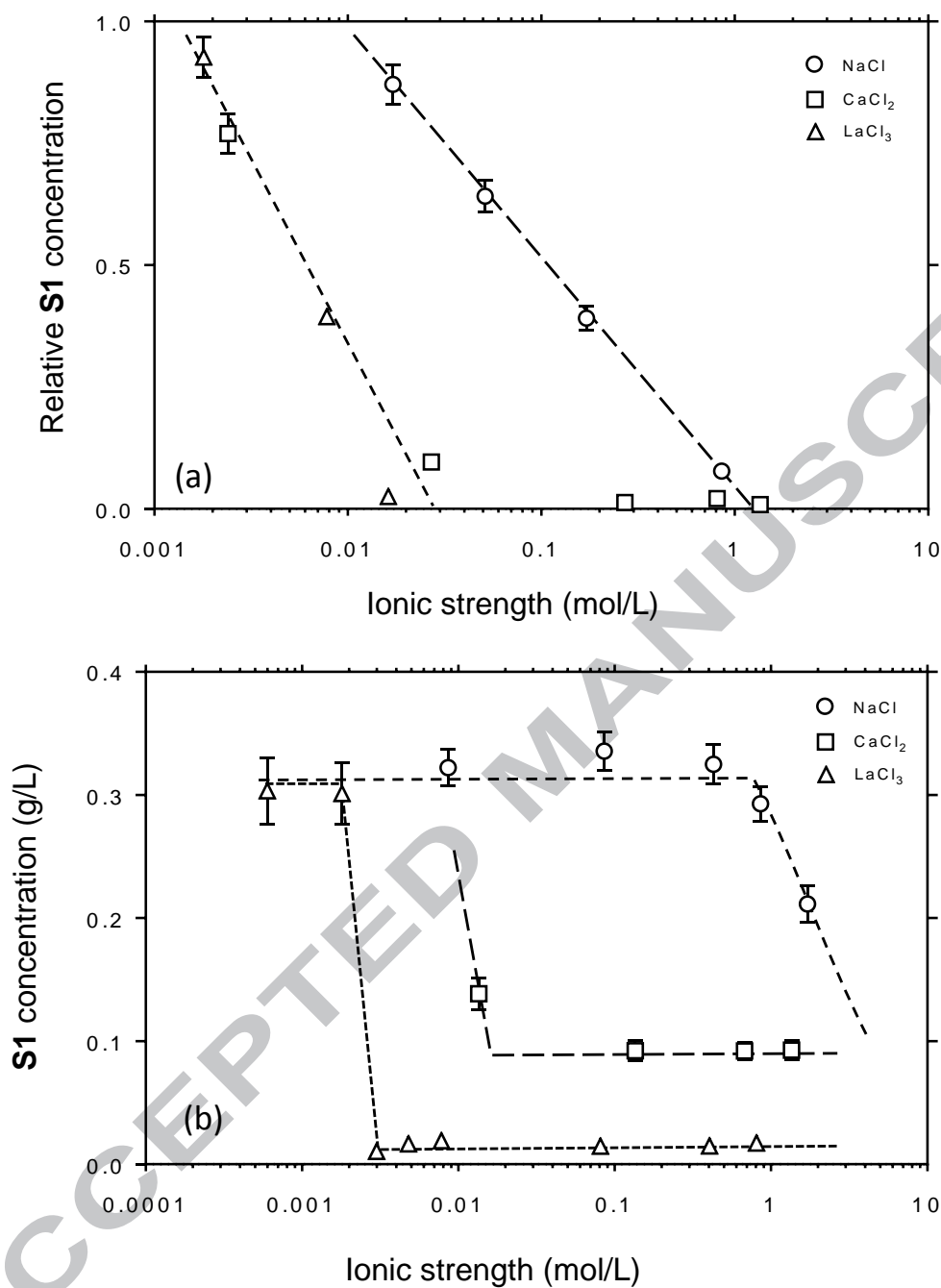
Fig. 5. (a) The effects of salt concentration on the dissolution of **S1** from HA. **S1** concentrations are relative to dissolution in deionized water. (b) The effect of salt concentration on the precipitation of **S1** from 0.31 g/L aqueous solution. For both plots, the lines are to guide the eye.

25

3.3.2. S1 solution structure

On the basis of the foregoing, we were interested to consider further the structure of **S1** as an anionic colloid. Small pieces (~1 cm^2) of freshly-cleaved muscovite mica were placed in two different **S1** solutions at low (~0.5 g/L) and high (~6 g/L) concentration for ~1 h (corresponding to the labeled positions *a* and *b*, respectively, in Fig. 1(a)). The mica pieces were then removed, rinsed with deionized water, and air-dried. Subsequent AFM measurements produced the images shown in Fig. 6, the adsorbed layer derived from the lower concentration solution at position *a* in Fig. 1(a) having a smoother, globular appearance compared to the higher concentration image from position *b*. This is more obvious from the respective section profiles also shown in Fig. 6. The higher concentration solution produced much smaller individual topological features which are similar to those reported elsewhere for the same type of commercial material [54,55], although in the latter studies the solutions were prepared using different procedures, and were of lower concentration (0.1 g/L). Thus, Liu et al. [55] started with commercial NaHA which was dissolved in water and subjected to a precipitation-ultrafiltration process to remove impurities and constrain the molecular weight range to between 5000 and 10000 Da; this produced AFM heights for adsorbed HA of 3.1–3.7 and 4.2–5.7 nm depending on the drying regime applied during sample preparation.
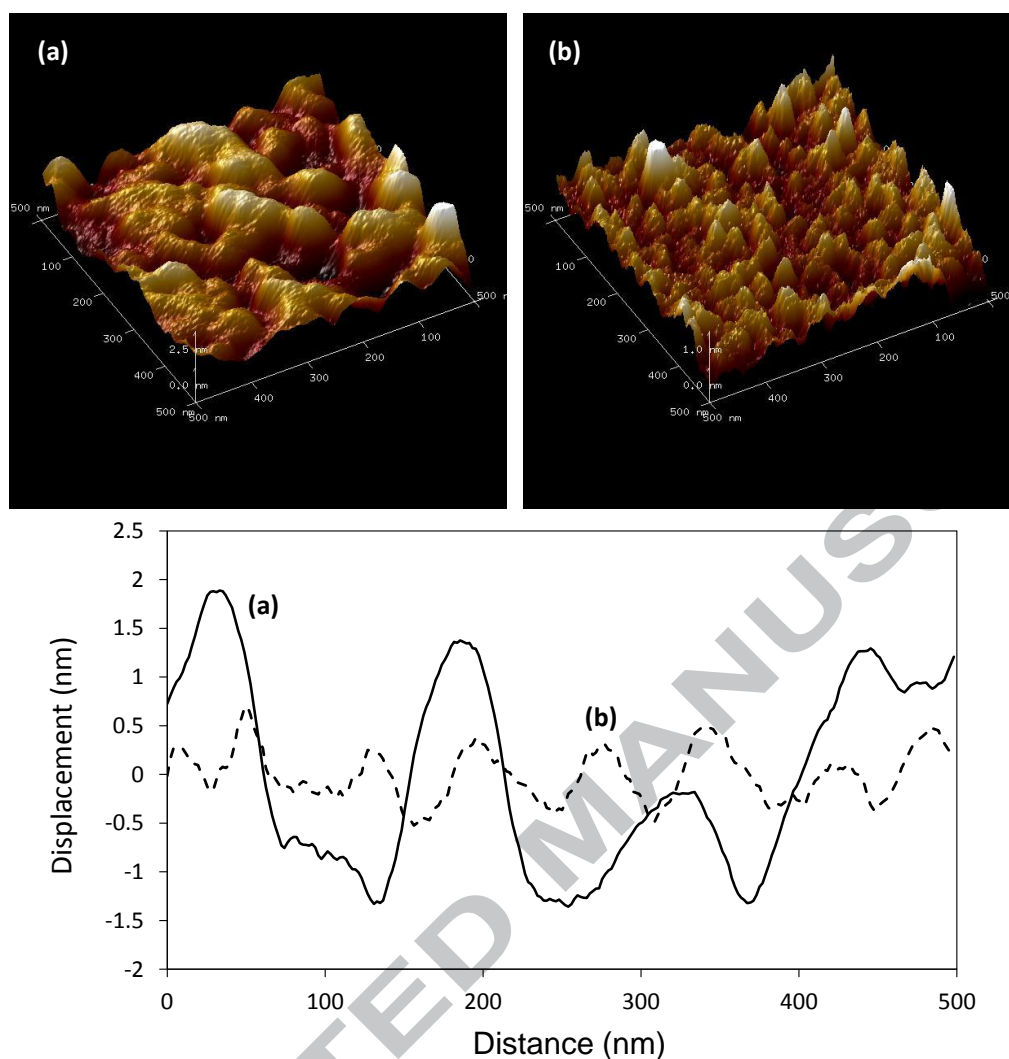
Fig. 6. Tapping mode 3-D topological AFM images (top) and section profiles through the respective AFM images (bottom) for mica containing adsorbed **S1** from (a) ~0.5 g/L and (b) ~6 g/L solutions in deionized water (see also Fig. 1(a) for the solutions used).

Pläschke et al. [54] purified Aldrich NaHA according to the method of Kim et al. [56] by dissolution in 0.1 mol/L NaOH in the presence of sodium fluoride (0.2 g/g HA). After several precipitation/re-dissolution (NaOH)/re-precipitation cycles, the resultant HA was adsorbed on mica surfaces at different pHs and imaged using AFM. The smallest particle diameters were found to be in the range 8-13 nm by AFM, compared with spheroids of 9–12 nm diameter

observed by transmission electron microscopy (TEM) [57]. Chen et al. [58] also observed similar images to those presented here for HA from an unidentified source.

On the other hand, Balnois et al. [59] studied two standard HAs: Suwannee River HA (SRHA; International Humic Substances Society) and a peat-derived HA (PHA; UK Geological Survey). These were sufficiently soluble in deionized water, and were free from non-HA impurities. For SRHA the observed pH-invariant AFM image height was 0.5−2 nm, whereas for the more hydrophobic PHA aggregated structures (~22 nm) dominated, with a smaller fraction of 1−3 nm.

With the above studies as background information, it is evident that the present results for **S1** adsorbed on mica show characteristics similar to those seen for other HA samples, including some that had been exhaustively purified. At our lowest concentration (albeit higher than in some previous studies), Fig. 6 (position *a*) is consistent with extended molecules present on the mica surface under the low ionic strength/neutral pH conditions, resulting in the uniform build-up of surface layers [55]. However, the image in Fig. 6 (position *b*) produced at higher **S1** concentration indicates the presence of smaller adsorbed units exhibiting more regular, distinct structures. Both images are also consistent with recent adsorption studies as a function of concentration on highly-ordered pyrolytic graphite [60] as well as with modeling [61].

However, as was helpfully pointed out by one referee, AFM images of this type refer only to films built up by dried primary units, and are not necessarily representative of the structure in solution. It was also suggested that SAXS measurements, for example, could provide additional information in support of solution structure, particularly if the dispersed units are colloidal, and a brief study of **S1** and **S2** solutions is therefore included here.

SAXS allows the probing of different dimensional characteristics of a system as a function of the scattering vector, $q = (4\pi \sin\theta)/\lambda$, where 2θ is the scattering angle and λ is the X-ray wavelength. The approach we have taken here is, admittedly, relatively simplistic, in order to identify differences in scattering behavior of the soluble HA fractions. On a log-log scale, the Porod plots shown in Fig. 7 plots relate scattering intensity, $I(q)$ to the scattering vector, q for **S1** and **S2** solutions in deionized water. In essence, each scattering curve shows two distinct power law regions, in which $I(q) \propto q^{-d}$, where d is the Porod exponent. At high q (>1 nm^{-1}), the scattering is dominated by the internal molecular arrangements of the structural units. In the lower q range (0.04 nm < q < 0.4 nm in this case), larger, presumably aggregated, structural units dominate the scattering. Analysis of scattering from the largest length scale units was not possible owing to the limitation of the accessible q range. This also prevented a simple Guinier analysis, according to $I(q) \propto \exp(-R_g^2 q^2/3)$, where R_g is the radius of gyration, as the plots for **S1** and **S2** shown in Fig. S4 are not linear, indicating aggregation or insufficiently low q range.

With due consideration for the limitations associated with the analysis of SAXS data alluded to above, we analyzed the present results using the global unified scattering function [62-64] provided in SansView software (v. 2.1, University of Tennessee)[2]. This approach allows for both Guinier and power-law contributions to the scattering curve, and for **S1** and **S2**, two sets of (R_g,d) parameters were found to describe the scattering intensity over the q range studied. The global unified model fitting parameters obtained from SansView are given in Table 4.

---

[2] Later versions of this software are known as SasView.

Table 4. Fitting parameters from SAXS data based on the global unified model.

	S1 concentration		S2 concentration
	2.03 g/L	11.9 g/L	1.59 g/L
$R_g(1)$ (nm)	9.07	11.4	8.95
$R_g(2)$ (nm)	46.6 *	51.5 *	47.5 *
$d(1)$	1.22	1.25	1.72
$d(2)$	2.82	2.98	2.84

*These should be regarded as minimum sizes, as they will be limited by the lowest accessible q value.

On this basis, the fitting data indicate two scattering regions. At high q, the R_g value of ~10 nm and low Porod exponents for **S1**, suggest that the scattering units responsible are semi-flexible chains (with $1 < d < \frac{5}{3}$) [62,65]. For the **S2** solution, the higher d is characteristic of a mass fractal (for which $\frac{5}{3} < d < 3$) with a swollen chain structure [65] and the Porod exponent as defined above corresponds to the fractal dimension. Additionally, at low q, the larger scattering units of at least 50 nm for both **S1** and **S2** are also consistent with mass fractals, but here they consist of clustered network structures, for which $d \approx 3$ [65]. Fig. 7 contains a simple schematic representation of the solution structure of the two soluble fractions in solution, based on these SAXS characteristics. Thus, at the molecular level (high q), scattering arises from **S1** and **S2** chains (low d) with radii of gyration ~10 nm. This is a value similar to the characterization length of 7.8 nm obtained by Shang and Rice for HA dissolved in alkaline solution [66]. Probing the solution structure on a greater length scale at low q identifies larger mass fractal scattering units with R_g ~50 nm, although here, this value will be governed by the lowest q value used in the analysis since a true Guinier region has not been attained. It can be seen from Fig. 6, that these dimensions are not reflected in the AFM image height (z-axis), mainly as a result of the relatively concentrated solutions saturating the mica surfaces, thereby obscuring the $z = 0$ position. On the other hand, the section taken in

the *xy* plane, also shown in Fig. 6, indicates the spatial dimensions of assumed close-packed adsorbed units to be ~100 nm and ~50 nm for 0.5 and 6 g/L, respectively. This is consistent with results from other AFM [54] and TEM [57] studies. Based on Porod log-log fits to scattering data, other workers have obtained *d* values between 2.2-2.4 for different humic substances in alkaline solution [66-68]. Osterberg and Morton also estimated from a SANS analysis an average cluster size of ~50 nm for two different HAs, and an R_g value of 32 nm for one of them [68].
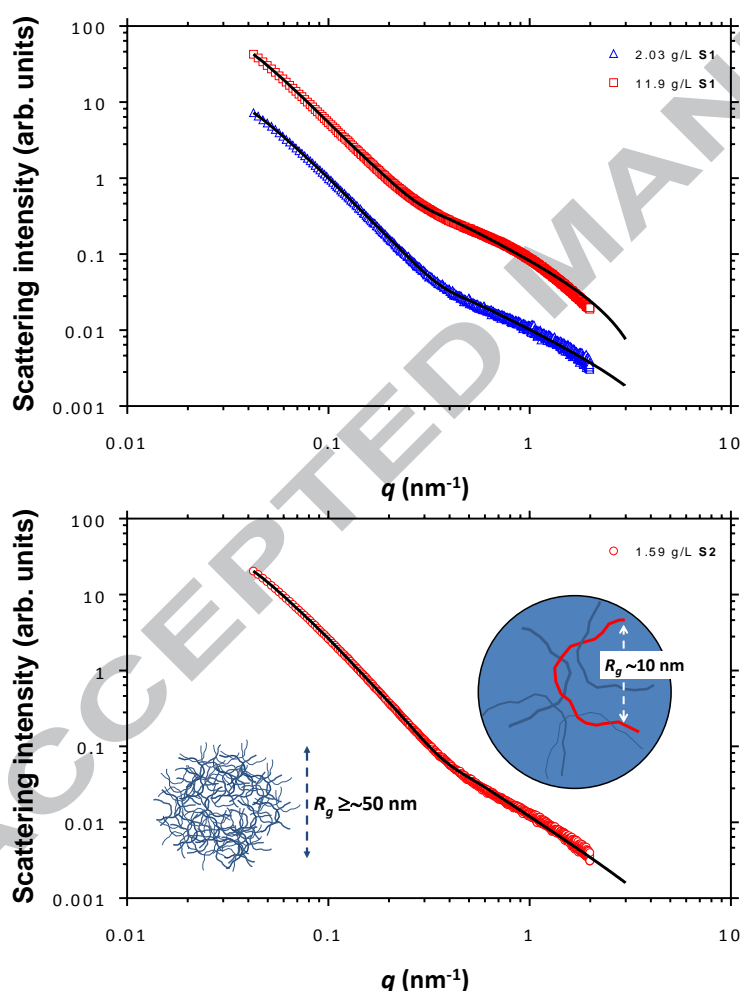

Fig. 7. SAXS Porod plots for **S1** (upper) and **S2** (lower) solutions at the indicated concentrations in deionized water. The solid lines are unified (power law and Guinier) fits to the data (see text for details). The lower plot also contains schematic representations of the length scales probed by the SAXS measurements.

3.4. Implications for the colloidal structure of HA

Characterization of the solubility fractions in the present work has revealed very significant structural differences between the soluble and insoluble fractions on the basis of TGA, elemental analysis, and infrared and solid-state ^{13}C NMR spectroscopy. The latter spectroscopic data indicate that **S1** and **S2** are structurally similar, with molecular weight and acid/base properties [69] likely to account for their respective solubility behavior. However, differences between **S1** and **S2** and their insoluble counterparts **I1** and **I2** are more significant. CPMAS ^{13}C NMR spectroscopy reveals higher aromaticity in the soluble species. This is reinforced by TGA results which indicate relatively higher aromatic content in the soluble fractions, and infrared spectroscopy which identifies lower levels of polysaccharide in **S1** and **S2**.

As described earlier, there have been numerous fractionation studies on HAs, and the specific species obtained from a particular HA would be expected to be dependent on the fractionation method used. Herein, HA fractionation on the basis of water solubility has led us to some considerations regarding HA structure, but it also provides further evidence for their colloidal nature. Although the present findings will apply particularly to the commercial HA sample studied, the wider application to other humic substances should also be considered. Soluble HA fractions at near-neutral pH conditions are likely to have important functions in soils, for example, including the regulation of ionic composition and determining the surface chemistry of minerals.

As already considered above, the structure of humic substances in general, and HAs in particular, has been the subject of debate over the years. The earliest models regarded humic materials as random coil ionic polymers, the conformation of which responded to their

environmental conditions of pH and electrolyte concentration (e.g. [70]). Subsequently, Wershaw [71,72] suggested a "membrane-micelle" model in which mixed micelles are formed from an ordered aggregation of plant-derived lipids and charged amphiphilic molecules held together by hydrogen bonding and π-π interactions. More recently, a consensus is developing that humic substances are supramolecular systems [22,23]. The building blocks involved in such suprastructures originate from smaller heterogeneous species derived from aromatic lignins, polysaccharides, proteins and lipids [22,73], evidence for which is present in the fractions derived in the present work. Each of these components exhibits different polarity/solubility characteristics, but their structures allow for mutual interactions, as proposed, for example, in the lignin-carbohydrate complex (LCC) model [74] and through interactions between lipids and "humic-like fractions", creating what the authors term a "structure-within-a-structure architecture" [13,75].

Through its behavior in water, the HA sample of the present study has been shown, both here and elsewhere [69], to be a multi-component mixture of species classes which are not covalently bonded, also supporting separation on the basis of adsorption [21] and ultrafiltration [19,20].

The colloidal character of HAs has been identified by AFM by a number of workers [1,54-59] although to the best of our knowledge this is the first time that such an HA sub-fraction has been imaged by AFM. The topological features of the **S1** fraction indicates a relatively small size for adsorbed units on mica, which is seen to be concentration dependent (Fig. 6), with the higher concentration producing the smaller-sized units. In part, the SAXS analyses agree with the AFM findings based on data at low q, from which the scattering units in **S1** and **S2** are suggested to have radii of gyration of at least 50 nm. In the high q region, the scattering from R_g ~10 nm units is consistent with the characteristic length determined by

33

Shang and Rice for HA molecules in alkaline solution [66]. Here, we propose that this latter dimension is characteristic of the constituents of the larger aggregated structures.

We have also focused mainly on the colloidal properties of **S1**, which has the highest water solubility. In respect of its sensitivity towards flocculation in the presence of indifferent cations, **S1** exhibits the classical properties of an anionic colloid, as also found for a purified HA sample in the presence of Mg^{2+} by Wang et al. [76].

4.   CONCLUSIONS

The nature of humic substances continues to be the subject of ongoing investigations, but it is only relatively recently that the supramolecular association of heterogeneous species has been generally accepted as defining their structural organization [22,23]. The result is that humic substances are multicomponent colloidal systems, the dispersed phase comprising a diverse range of self-assembled components, building on the membrane-micelle model of Wershaw [71,72]. In the present work we have fractionated a commercial HA sample by sequential dissolution in deionized water and shown that one of the sub-fractions, in particular, behaves as a hydrophilic anionic colloid. AFM and SAXS measurements suggest an approximate size for the colloidal dimensions. The results lend some support for Lehmann and Kleber's "emergent view" of the nature of humic substances inasmuch as we have identified water-soluble "forms that are actually soluble in water" [11]. The results also provide a link with the earlier "polymer model" in which humic substances were considered as ionic polymers [77].

We have used a multi-technique approach to the study of the composition and colloidal properties of a commercial sample of HA. As reported previously by others [24,25], we also

observed unusual solubility behavior of this HA sample, which enabled us to isolate four fractions by sequential dissolution under near-neutral pH conditions – two water-soluble products (**S1** and **S2**) and two water-insoluble residues (**I1** and **I2**). Although not carried out here, it is possible that a more exhaustive separation scheme, perhaps including pH and ionic strength variation, would lead to a greater number of narrower class fractions as are being studied by Klučáková and her coworkers [78-81].

The analytical results highlight significant differences between the soluble and insoluble HA fractions. The former contain proportionally more oxygen (revealed by a combination of elemental analysis and TGA), with increased carbonyl functionality (>C=O evident from ^{13}C CPMAS NMR and ATR-IR) and phenol groups (aromatic C-OH from ATR-IR). Additionally, the soluble fractions contain a greater aromatic/aliphatic carbon ratio (from ^{13}C CPMAS NMR and TGA) and a lower polysaccharide C-O content (ATR-IR). Thus, the components identified here are consistent with known structural features in all HAs.

As pointed out by Tarasevich et al. [1], to date there have been relatively few systematic investigations of the effects of concentration on the form taken by HA in solution. However, using a simple dissolution approach, we have shown that the original commercial humic acid used in the present study contains non-covalently bonded species with different polarity and water solubility. In this way, the present findings concur with the description of HA as a supramolecular system, with macromolecules as well as molecular aggregates being present, as concluded by Baigorri et al. [82].

ACKNOWLEDGEMENTS

REFERENCES

[1]   Y.I. Tarasevich, S.A. Dolenko, M.Y. Trifonova, E.Y. Alekseenko, Colloid J. 75 (2013) 207-213.

[2]   R. von Wandruszka, Geochem. Trans., 1 (2000) 10-15.

[3]   L. Gutierrez, M. Pawlik, Int. J. Min. Proc., 126 (2014) 117–125.

[4]   L. Gutierrez, M. Pawlik, Int. J. Min. Proc., 126 (2014) 126–135.

[5]   J.L. Margeson, V. Hornof, G.H. Neale, J. Can. Pet. Tech., 28 (1989) 57-62.

[6]   L.S. Kotlyar, B.D. Sparks, H. Kodama, P.E. Grattan-Bellew, Energy Fuels, 2 (1988) 589-593.

[7]   M. Ishiguro, W. Tan, L.K. Koopal, Colloids Surfaces, A 306 (2007) 29.

[8]   I. Christl, R. Kretzschmar, Environ. Sci. Technol., 41 (2007) 1915-1920.

[9]   L.K. Koopal, T.P. Goloub, T.A. Davis, J. Colloid Interface Sci. 275 (2004) 360-367.

[10]   P. Conte, A. Agretto, R. Spaccini, A. Piccolo, Environ. Poll., 135 (2005) 515–522.

[11]   J. Lehmann, M. Kleber, Nature, 528 (2015) 60-68.

[12]   T.F. Guetzloff, J.A. Rice, Science Total Environ., 152 (1994) 31–35.

[13]   G. Chilom, A.S. Bruns, J.A. Rice, Org. Geochem., 40 (2009) 455–460.

[14]   C. Young, R. von Wandruszka, Geochem. Trans., 2 (2001) 16-20.

[15]   L.M. Yates, R.R. Engebretson, T.J. Haakenson, R. von Wandruszka, Anal. Chim. Acta, 356 (1997) 295-300.

[16]   A. Nebbioso, A. Piccolo, Anal. Bioanal. Chem., 405 (2013) 109–124.

[17]   H.K.J. Powell, R.M. Town, Anal. Chim. Acta, 267 (1992) 47–54.

[18]   P. Conte, R. Spaccini, D.Smejkalova, A. Nebbioso, A. Piccolo, Chemosphere, 69 (2007) 1032–1039.

[19]   L. Carlsen, P. Lassen, P. Warwick, A. Randall, Chemosphere, 33 (1996) 659-670.

[20]   O. Francioso, S. Sánchez-Cortés, D. Casarini, J.V. Garcia-Ramos, C. Giavatta, C. Gessa, J. Mol. Struct. 609 (2002) 137-147.

[21]   A. Pitois, L.G. Abrahamsen, P.I. Ivanov, N.D. Bryan, J. Colloid Interface Sci., 325 (2008) 93–100.

[22]   A. Piccolo, Soil Sci., 166 (2001) 810-832.

[23]   R. Sutton, G. Sposito, Environ. Sci. Technol., 39 (2005) 9009-9015.

[24]   M. Klučáková, M. Pekař, Colloids Surfaces, A 252 (2005) 157–164.

[25]   M. Klučáková, M. Pekař, Colloids Surfaces, A 318 (2008) 106–110.

[26]   C. Gamboa, A.F. Olea, Colloids Surfaces, A 278 (2006) 241–245.

[27]   M. De Nobili, M. Contin, L. Leila, Can. J. Soil Sci., 70 (1990) 531-536.

[28]   R.L. Johnson, K. Schmidt-Rohr, J. Magn. Reson., 239 (2014) 44–49.

[29]   R.M.B.O. Duarte, A. C. Duarte, Atmospheric Environ., 42 (2008) 6670–6678.

[30]   V.I. Esteves, A.C. Duarte, Marine Chem., 63 (1999) 225–233.

[31]   R.L. Malcolm, P. MacCarthy, Environ. Sci. Technol., 20 (1986) 904-911.

[32]   F.J. Stevenson, K.M. Goh, Geochim. Cosmochim. Acta, 35 (1971) 471-483.

[33]   A.L. Mafra, N. Senesi, G. Brunetti, A.A.W. Miklós, A.J. Melfi, Geoderma, 138 (2007) 170–176.

[34]   J. Polak, M. Bartoszek, M. Ządło, A. Kos, W.W. Sułkowski, Chemosphere, 84 (2011) 1548–1555.

[35]   M. Tatzber, M. Stemmer, H. Spiegel, C. Katzlberger, G. Haberhauer, A. Mentler, M.H. Gerzabek, J. Plant Nutr. Soil Sci., 170 (2007) 522–529.

[36]   A. Piccolo, F.J. Stevenson, Geoderma, 27 (1982) 195–208.

[37]   D.C.W. Tsang, N.J.D. Graham, I.M.C. Lo, Chemosphere, 75(2009) 1338–43.

[38]   P. Innocenzi, J. Non-Cryst. Solids, 316 (2003) 309–319.

[39]   M. Fuentes, R. Baigorri, G. González-Gaitano, J.M. García-Mina, Org. Geochem., 38 (2007) 2012–2023.

[40]   F. Monteil-Rivera, E.B. Brouwer, S. Masset, Y. Deslandes, J Dumonceau, Anal. Chim. Acta, 424 (2000) 243–255.

[41]   R.L. Johnson, K. Schmidt-Rohr, J. Magn. Res., 239 (2014) 44–49.

[42]   A. Majid, J.A. Ripmeester, Fuel, 69 (1990) 1527-1536.

[43]   H.-S. Shin, J.M. Monsallier, G.R. Choppin, Talanta, 50 (1999) 641–647.

[44]   N.A. Wall, G.R. Choppin, Appl. Geochem., 18 (2003) 1573–1582.

[45] K. Hayase, H. Tsubota, Geochim. Cosmochim. Acta, 47 (1983) 947–952.

[46] M. Terashima, M. Fukushima, S. Tanaka, Colloids Surfaces, A 247 (2004) 77–83.

[47] R.R. Engebretson, R. Von Wandrusrka, Environ. Sci. Technol., 28 (1994) 1934–1941.

[48] A. Piccolo, D. Smejkalova, Environ. Sci. Technol., 42 (2008) 699–706.

[49] M. Fukushima, S. Tanaka, K. Hasebe, M. Taga, H. Nakamura, Anal. Chim. Acta, 302 (1995) 365-373.

[50] J. Lyklema, Colloids Surfaces, A 460 (2014) 468–472.

[51] J. Lyklema, J. Colloid Interface Sci., 392 (2013) 102–104.

[52] K. Furukawa, Y. Takahashi, Chemosphere, 73 (2008) 1272–1278.

[53] T.A. Sabirjanovna, S. Pasa, D.U. Zhumasilovich, H. Temel, N.G. Oryntayevna, Desal. Water Treatment, 57 (2016) 776–790.

[54] M. Pläschke, J. Römer, R. Klenze, J.I. Kim, Colloid Surfaces, A 160 (1999) 269–279.

[55] A. Liu, R.C. Wu, E. Eschenazi, K. Papadopoulos, Colloids Surfaces, A 174 (2000) 245–252.

[56] J. I. Kim, G. Buckau, G. H. Li , H. Duschner, N. Psarros, Fresenius J. Anal. Chem., 338 (1990) 245-252.

[57] S.C.B. Myneni, J.T. Brown, G.A. Martinez, W. Meyer-Ilse, Science, 286 (1999) 1335-1337.

[58] C. Chen, X. Wang, H. Jiang, W. Hu, Colloids Surfaces, A 302 (2007) 121-125.

[59] E. Balnois, K.J. Wilkinson, J.R. Lead, J. Buffle, Environ. Sci. Technol., 33 (1999) 3911-3917.

[60] Z. Liu, Y. Zu, R. Meng, Z. Xing, S. Tan, L. Zhao, T. Sun, Z. Zhou, Microscopy Microanal., 17 (2011) 1015-1021.

[61] L.T. Sein, J.M. Varnum, S.A. Jansen, Environ. Sci. Technol., 33 (1999) 546-552.

[62]   G. Beaucage, J. Appl. Cryst. 28 (1995) 717-728.

[63]   G. Beaucage, J. Appl. Cryst. 29 (1996) 134-146.

[64]   G. Beaucage, H.K. Kammler, S.E. Pratsinis, J. Appl. Cryst. 37 (2004) 523-535.

[65]   B. Hammouda, J. Appl. Cryst. 43 (2010) 1474-1478.

[66]   C. Shang, J.A. Rice, J. Colloid Interface Sci., 305 (2007) 57–61.

[67]   J.A. Rice, E. Tombàcz, K. Malekani, Geoderma, 88 (1999) 251-264.

[68]   R. Osterberg, K. Mortensen, Eur. Biophys. J., 21 (1992) 163-167.

[69]   M. Klučáková, React. Functional Polymers, 109 (2016) 9–14.

[70]   M.M. Kononova, Soil Organic Matter. Its Nature, Its Role in Soil Formation and in Soil Fertility. Pergamon Press, New York, 1961.

[71]   R.L. Wershaw, Env. Health Perspect., 83 (1989) 191-203.

[72]   R.L. Wershaw, US Geological Survey Water-Supply Paper, 1994, Vol.2410.

[73]   K.H. Tan, Humic Matter in Soil and the Environment. Principles and Controversies, CRC Press, Boca Raton, 2nd Edition, 2014, Chaps. 2 and 5.

[74]   C. Colombo, G. Palumbo, R. Angelico, H.G. Cho, O. Francioso, A. Ertani, S. Nardi, Chemosphere, 138 (2015) 821–828.

[75]   G. Chilom, A. Baglieri, C.A. Johnson-Edler, J.A. Rice, Org. Geochem., 57 (2013) 119–126.

[76]   L.-F. Wang, L.-L. Wang, X.-D. Ye, W.-W. Li, X.-M. Ren, G.-P. Sheng, H.-Q. Yu, X.-K. Wang, Environ. Sci. Technol., 47 (2013) 5042−5049.

[77]   F.J. Stevenson, Humus Chemistry: Genesis, Composition, Reactions, 2nd Edition, John Wiley & Sons, Ltd, New York, 1994.

[78]   M. Klučáková, R. Kolajová, React. Funct. Polymers, 78 (2014) 1–6.

[79]   M. Klučáková, M. Kalina, J. Soils Sediments, 15 (2015) 1900-1908.

[80]   M. Klučáková, Environ. Sci. Pollut. Res, 23 (2016) 7722–7731.

[81]   M. Klučáková, React. Funct. Polymers, 109 (2016) 9–14.

[82]   R. Baigorri, M. Fuentes, G. González-Gaitano, J.M. García-Mina, Colloids Surfaces, A 302 (2007) 301–306.

R_g ~10 nm

Molecular interactions: characteristic length

Humic acid soluble fraction: aggregate size

$R_g \geq$ ~50 nm

42